8-24-2022

Upcycling Mask Waste to Carbon Capture Sorbents: A Combined Experimental and Computational Study

Mark Robertson

Alejandro Guillen Obando

Bianca Nunez

Haoyuan Chen

Zhe Qiang

Article

Upcycling Mask Waste to Carbon Capture Sorbents: A Combined Experimental and Computational Study

Mark Robertson,[§] Alejandro Guillen Obando,[§] Bianca Nunez, Haoyuan Chen,* and Zhe Qiang*

Cite This: https://doi.org/10.1021/acsaenm.2c00030

Read Online

ACCESS | 📊 Metrics & More | 📖 Article Recommendations | 🔵 Supporting Information

ABSTRACT: Massive plastic pollution and grand scale emission of CO_2 into the atmosphere represent two major and deeply connected societal challenges, which can have adverse impacts on climate, human health, and marine ecosystems. In particular, the COVID-19 pandemic led to substantially increased production, use, and discarding of disposable masks, a problem that requires urgent and effective technological solutions to mitigate their negative environmental impacts. Furthermore, over the years significant research efforts have sought to address the challenges of plastic waste and CO_2 emission, such as development of chemical upcycling methods and low-cost CO_2 capture sorbents at scale, respectively. In this work, we introduce a simple and scalable method for directly converting surgical polypropylene mask waste into sulfur-doped carbon fibers, which can exhibit a high CO_2 sorption capacity of ≤ 3.11 mmol/g and high selectivity (>45) against N_2 gas. This excellent performance is attributed to the high affinity between sulfur heteroatoms in the carbon framework and CO_2 gas molecules, confirmed by combined experimental and simulation investigations. This work provides an industrially viable approach for upcycling plastic waste into carbon-based products with increased value, which can then be employed to address the environmental challenges of CO_2 remediation.

KEYWORDS: plastic upcycling, CO_2 sorbents, doped carbon, carbon fibers, DFT calculations
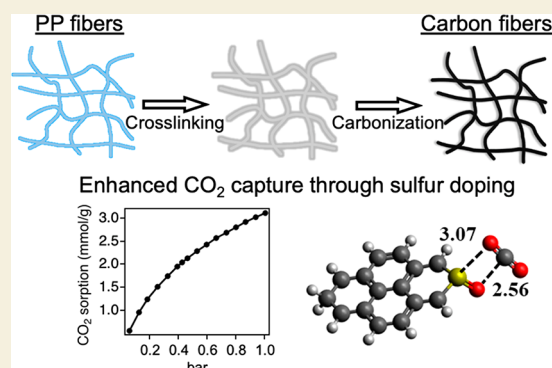
1. INTRODUCTION

Massive greenhouse gas emission from various sectors, including electricity generation, transportation, and manufacturing, has resulted in severe negative impacts on the planet, such as accelerated global warming, extreme weather, and respiratory disease from air pollution.[1-3] In particular, a constant increase in the atmospheric carbon dioxide (CO_2) concentration would eventually leave society on the verge of potential environmental and health crises.[4,5] It is undoubtedly crucial to build pathways to reduce the emission of CO_2 and create a carbon-negative economy, as established in the Paris Agreement, addressing significant challenges that are linked to climate change.[6] This urge has led to tremendous efforts to develop different CO_2 capture technologies, including sorbents for capturing CO_2 in its postcombustion state as well as direct air capture.

Liquid sorbent systems for removing CO_2 from manufacturing plants have been successfully demonstrated and adopted at commercial scales but are often challenged by the production of harmful byproducts, corrosion, and large energy penalties for spent sorbent regeneration. An alternative to liquid sorbent-based technologies is using solid sorbents that would rely on physical and/or chemical adsorption to capture CO_2. These systems can provide high adsorption capacity and high selectivity toward CO_2 in mixed gas streams, with potential of

having a relatively low cost and requiring a low level of energy consumption for sorbent regeneration. One of the leading technologies in this area is associated with metal organic frameworks (MOFs). These nanoporous materials are developed by the assembly of metal ions with organic ligands,[7] which can produce tunable pore structures and a framework identity, as well as large surface areas. These features allow their high sorption capacity and the ability to store CO_2 for extended periods of time.[8] Notably, a recent work from Lin et al. detailed the scalable production of a zinc-based MOF that demonstrated excellent CO_2 adsorption capacities, even in mixed gas streams with $\leq 40\%$ relative humidity. The sorbents exhibited excellent cycle stability beyond 450 000 cycles due to the durability of the material and small energy penalty to regenerate the sorbent. In addition to MOFs, many other porous materials have been demonstrated as solid sorbents for CO_2 capture, including but not limited to carbons,[9,10] polymers,[11] covalent organic frameworks,[12] silica,[13] zeo-

lites,[14,15] and metal oxides.[16] In particular, the synthesis of porous carbon for CO_2 capture has attracted significant interest because of its excellent stability at high temperatures in the presence of water vapor.[17] In 2013, Hao et al. prepared activated carbons using hydrothermally carbonized biomass, which has a surface area of 841 m^2/g and a CO_2 uptake of 1.45 mmol/g under 0.1 bar at 25 °C.[18] Similarly, Li et al. developed CO_2 sorbents through carbonization of biomass precursors and subsequent chemical activation using potassium hydroxide (KOH) to enhance surface areas.[19] The materials exhibited CO_2 adsorption capacities of ≤4.36 mmol/g at 25 °C and 1 bar, due to their large surface areas of 3337 m^2/g. While these sorbents, including MOFs and porous carbons, demonstrate great material performance as CO_2 sorbents, there are some limitations on their potential widespread use and commercial viability. For example, many processes for producing MOFs require expensive precursors and multiple synthetic steps and are limited to small production batch sizes that are currently a challenge in matching industrial requirements and/or needs for CO_2 capture. Similarly, the production of activated carbons can require additional functionalization or activation steps to enhance adsorption, which could result in increased cost, with additional concerns about potential supply chain challenges of biomass precursors. Alternatively, doping heteroatoms into the carbon matrix can also improve the CO_2 sorption capacity by enhancing the favorable interactions between the sorbate and sorbent. Specifically, the introduction of heteroatoms can improve the electronegativity of carbon frameworks, providing an important mechanism for improving CO_2 uptake compared to their undoped counterparts. For example, a recent study by Ma et al. designed nitrogen- and oxygen-enriched porous carbons (surface area of 1350 m^2/g) with CO_2 adsorption capacities of ≤4.33 mmol/g at 25 °C and 1 bar.[20] Similarly, a study by Saha et al. demonstrated that sulfur-doped mesoporous carbons (with the sulfur content ranging from 8.2 to 12.9 atom %) can have CO_2 sorption capacities higher than those of commercially available activated carbons.[21] This is because sulfur-containing functional groups, such as sulfonic acids and sulfides, can attract CO_2 via polar interactions.[22] Moreover, sulfur can be co-doped with other heteroatoms, as shown by Tian et al., who fabricated a nitrogen, sulfur co-doped carbon with nanoscopic honeycomb structures. Compared with that of nitrogen-doped carbon with the highest doping level, the co-doped material exhibited a slightly higher adsorption capacity (4.7 mmol/g compared to 4.5 mmol/g) while having a smaller micropore volume and lower nitrogen doping levels, suggesting that the enhancement in performance was attributed to the presence of the sulfur heteroatoms.[23] Given that many studies have indicated the advantage of sulfur doping in carbons for enhancing CO_2 adsorption capacity, a clear mechanistic and quantitative understanding of the favorable interactions between sulfur heteroatoms in the porous carbon framework and CO_2 at a molecular level would be useful for informing the rational design of doped carbon sorbents.[24,25]

In recent years, plastic industry has taken significant initiatives in reducing CO_2 emission through continued efforts in plastic recycling and upcycling. According to a study conducted by the U.S. Environmental Protection Agency (EPA) in 2016, transforming just 5% of plastic waste into recyclable materials would reduce greenhouse gas emissions by 10.2 million metric tons of carbon equivalent (MTCE).[26] Additionally, plastic recycling can also address other environ-

mental challenges such as microplastic formation in aqueous media, which is detrimental to the marine ecosystem and human health.[27] In general, two routes exist to address plastic waste, mechanical recycling and chemical upcycling. The first one relies on high-temperature and high-shear environments to reprocess plastic waste into new, typically downgraded products,[28] while the latter can chemically transform plastic waste into value-added products, such as fuels,[29] functionalized polymers,[30,31] and carbon materials.[32,33] Among them, conversion of commodity polymer waste into carbon is compelling because carbons have advantages of high electrical and thermal conductivity, chemical inertness, and excellent stability in non-oxidative environments, which are not present in polymeric materials. Therefore, such chemical upcycling routes significantly broaden the application scope of plastic waste as a feedstock. As an example, Pol et al. fabricated carbon materials using polyethylene (PE) plastic bags, which have yields of >50 wt %, and the resulting carbons contain porous structures with a surface area of 752.3 m^2/g.[34] These materials have been used as anodes in lithium-ion batteries in which they exhibited specific capacitances that were beyond the theoretical limit of using conventional graphite-based electrode materials. Furthermore, Wyss et al. have recently developed a robust method for producing carbon materials from various sources, including mixed plastic waste, without the requirement of solvent use, purification steps, or electrical furnaces.[35] Specifically, this method is known as flash Joule heating, which uses an electrical pulse and blackbody radiation to convert the source into a "flash graphene" product in as little as 10 ms. This flash Joule heating approach has been demonstrated to produce carbons with tunable material characteristics, including heteroatom doping levels and porosity, and holds great potential as a method for upcycling mixed plastic waste into carbon products.[36,37] Additionally, Hu and Lin demonstrated the use of polypropylene (PP) fibers to create hollow carbon fibers, followed by an activation step to create micropores.[38] Importantly, this work can address the massive amounts of mask waste produced during the COVID-19 pandemic, which has resulted in substantially increased production and usage of PP-derived single-use plastics. A study in late 2021 by Roberts et al. reported an 80-fold increase in pollution caused by masks (most are made of PP) since the start of the pandemic, increasing its pollution population from 0.01% to 0.8%.[28] Similarly, an article published through the United Nations estimated that 87 000 tons of mask waste was disposed between March 2020 and November 2021.[39] Masks not only act as a landfill pollutant but also present a risk as micropollutants and require the development of alternative recycling and/or upcycling methods to mitigate their negative effects on the environment.[40] Recently, we demonstrated the production of multifunctional carbon fibers derived from PP-based surgical masks.[41] The products exhibited potential uses in Joule heating, oil cleanup, and water purification. However, a postactivation step is needed to enable efficient water remediation sorbents from fibril PP precursors, which could introduce additional cost for scaled production. Moreover, as previously discussed, establishing a robust technology to simultaneously address challenges in plastic waste management and CO_2 capture, two deeply interconnected environmental issues, would be highly desirable. In previous studies, various techniques have been developed to upcycle plastic waste precursors, including polyethylene terephthalate and poly-ethylene, to carbon capture sorbents, achieving high CO_2

Scheme 1. Structures of All of the Molecules Considered in the Computational Work
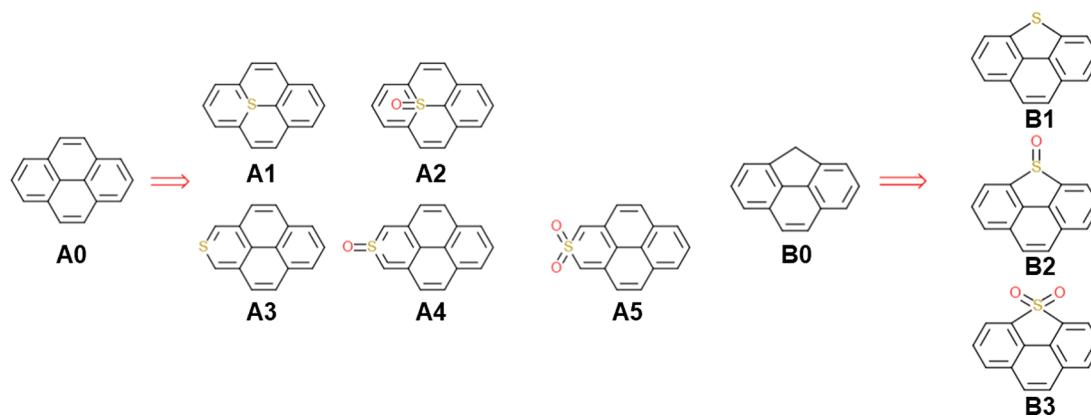
adsorption capacities of 4.58 and 3.80 mmol/g, respectively.[42,43] However, these processes have low degrees of carbon yield (<30 wt %) and require activation through exposure to potassium hydroxide, which adds complexity to processing steps and can reduce the ability to produce sorbents at commercially relevant scales.

Herein, we employ sulfonation-based chemistry to crosslink PP fibers from surgical masks, adding sulfonic acid groups to the polymer backbone, and further convert them into sulfur-doped (S-doped) carbon fibers. The presence of sulfur enables these fibers to have a high sorption capacity of ≤ 3.11 mmol/g of CO_2 at 25 °C and 1 bar. Additionally, the influence of S doping on the adsorption behaviors of carbon fibers is systematically studied by combined experimental and computational investigations. Our simple method can be easily scaled up to convert large scale mask waste into CO_2 sorbents, providing an industrially feasible pathway for upcycling of plastic waste into products that directly address environmental threats such as greenhouse gases and other toxic chemicals.

2. METHODS

2.1. Materials

Sulfuric acid (98 wt %) was purchased from Thermo Fisher. Surgical masks composed of PP fibers used throughout this work were purchased from CVS Health. Deionized (DI) water was obtained using a Milli-Q IQ 7003 ultrapure lab water purification system.

2.2. Preparation of Sulfur-Doped Carbon Fibers

Surgical masks were first cut into small pieces to retrieve nonwoven outer layers for this study. The mask pieces (0.3 g) were then introduced into a 100 mL glass beaker, and 30 mL of 98% sulfuric acid was added. A glass slide was placed on top of the mask pieces ensuring they were fully submerged. These materials were then heated at 145 °C using a Thermo Scientific electric muffle furnace. After reaction, mask pieces were carefully removed from the beaker and washed at least three times using DI water. Subsequently, the mask pieces were placed in a vacuum oven to dry overnight to remove residual water. These samples were then carbonized in a tube furnace (MTI Corp., OTF-1200x), using a heating ramp of 5 °C/min to 800 °C under a N_2 atmosphere.

2.3. Characterization of Materials

The chemical compositions of mask samples were determined using a PerkinElmer Frontier attenuated total reflection Fourier transform infrared (FTIR) spectrometer. The scan range was $4000-600$ cm^{-1} with averaging over 32 scans and a resolution of 4 cm^{-1}. A Zeiss Ultra 60 field-emission scanning electron microscope (SEM) was utilized to characterize the microstructures of masks after different processing stages, including cross-linking and carbonization. Energy-dispersive X-

ray spectroscopy (EDX) was performed to understand the elemental composition of the carbonized masks. ImageJ was then used to measure fiber diameters after each processing step. A Micromeritics Tristar II instrument was used to determine CO_2 and N_2 sorption performance at ambient temperature. Additionally, pore textures of carbonized mask fibers were determined from the adsorption and desorption isotherms of N_2 at 77 K. Specifically, the pore size distribution was determined from the Barrett–Joyner–Halenda (BJH) model, while the surface area and pore size were obtained from Brunauer–Emmett–Teller (BET) analysis. X-ray photoelectron spectroscopy (XPS) experiments were performed using a Thermo Fisher ESCALAB Xi+ spectrometer equipped with a monochromatic Al X-ray source (1486.6 eV) and a MAGCIS Ar+/Arn+ gas cluster ion sputter gun. Binding energies were calibrated with respect to C 1s, at 284.8 eV. A high-resolution scan of cross-linked and carbonized fibers was performed to study the heteroatom content as well as their detailed chemical bond information, by using Thermo Avantage analysis software. A TA Q500 thermogravimetric analysis (TGA) instrument was used to characterize the adsorption–desorption capacity and cycle stability of optimized mask-derived carbon fibers for CO_2 capture.

2.4. Computational Methods

Density functional theory (DFT) calculations were employed to calculate the binding energy of CO_2 with representative structural motifs in the fiber. Two carbon-based aromatic molecules (denoted A0 and B0) and their S-containing derivatives (denoted A1–A5 and B1–B3) were constructed, as shown in Scheme 1. In the derivative molecules, different chemical environments of S were considered and both S-containing bonds identified via XPS (C–S–C and C–S–O) were included. The geometries of A0–A5 and B0–B3 molecules were drawn and optimized using the M06-2X density functional and def2-SVP basis set.[44,45] Subsequently, a CO_2 molecule was added to each molecule in several different orientations. Each complex structure was then optimized at the same level of theory but with the DFT-D3 dispersion correction to account for the van der Waals interaction between CO_2 and Ax/Bx molecules.[46,47] For each optimized complex structure, a counterpoise-corrected single-point energy calculation was performed using the same density functional and dispersion correction but a larger basis set (def2-TZVP) to further improve the accuracy of the electronic energy.[48–50] The binding energy between CO_2 and each Ax/Bx molecule at each binding mode was then obtained from this calculation. All of the calculations were performed using Gaussian16 revision A03.[51] For each molecule (A0–A5), we also carried out energy decomposition analysis for its lowest-energy binding mode to dissect the overall binding energy into the contribution from different types of intermolecular forces, using the symmetry-adapted perturbation theory (SAPT) method in the Psi4 package.[52,53] The SAPT0 level of theory together with the aug-cc-pVTZ basis set was used.[54–56] Cartesian coordinates of all of the optimized structures are provided as part of the Supporting Information.

Scheme 2. Illustration of the Processing Method for Converting PP Masks into Carbon Fibers
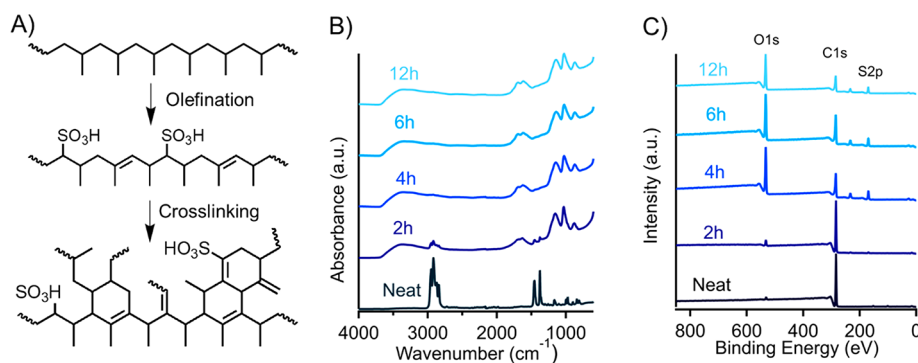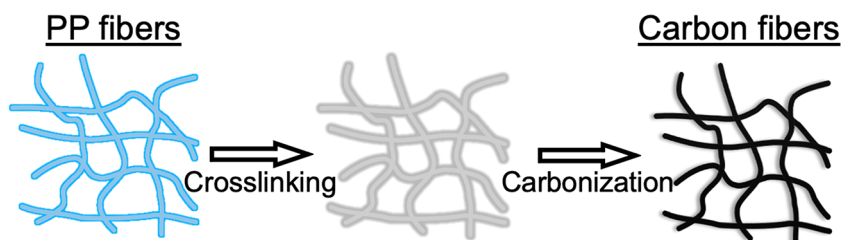
Figure 1. (A) Simplified cross-linking reaction mechanism of PP fibers, through sulfonation that enables the formation of cross-linked networks. (B) FTIR spectra of cross-linked PP fibers with an increasing sulfonation time. (C) XPS survey scan of cross-linked PP mask fibers with an increasing sulfonation time.
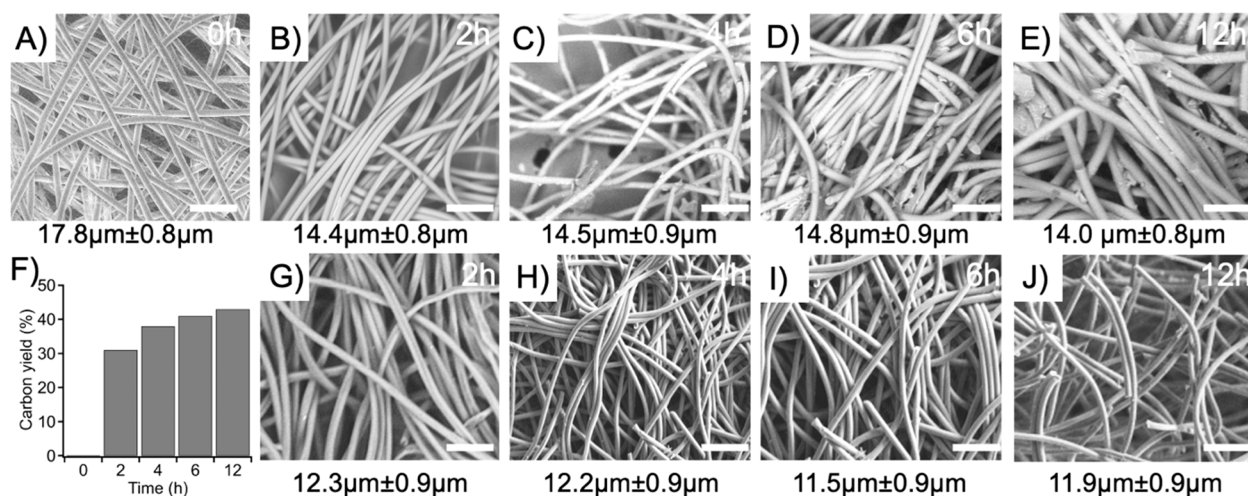

Figure 2. (A) SEM images of mask-derived PP fibers and after cross-linking for (B) 2, (C) 4, (D) 6, and (E) 12 h. (F) Carbon yield of PP fibers with an increasing crosslinking time. SEM images of carbon fibers with cross-linking times of (G) 2, (H) 4, (I) 6, and (J) 12 h. Scale bar of 100 μm.

3. RESULTS AND DISCUSSION

The synthesis of carbon fibers from PP-derived disposable masks is similar to that from a previous report,[41] heating mask pieces in concentrated sulfuric acid at increased temperatures to induce PP crosslinking, which is necessary for allowing high degrees of carbon yield after the carbonization process (Scheme 2). The sulfonation reaction of PP is represented through a simplified reaction scheme as shown in Figure 1A. Initially, sulfonic acid groups are introduced to the polymer backbone, which can dissociate homolytically to form double bonds through olefination. These bonds react further through secondary additions, rearrangements, and dissociations and ultimately form radical species that can undergo intermolecular coupling with other polymer chains. The involved mechanisms are very similar to those from several previous reports.[57,58]

This process is detailed in the FTIR spectra in Figure 1B, where characteristic peaks can be monitored as a function of sulfonation time. Specifically, the peak at 2920 cm^{-1} represents the C−H stretch of the polymer backbone that diminishes as the sulfonation reaction progresses. The intensity of these peaks first decreased after 2 h, indicating an incomplete crosslinking of PP fibers. After 4 h, these peaks completely disappeared. The peak at 3326 cm^{-1} corresponds to the hydroxyl groups of the sulfonic acid moieties introduced to the polymer backbone and is further evidence of the sulfonation reaction. Additionally, the formation of alkenes is represented by the peak at 1604 cm^{-1} and the formation of sulfonic acid groups is evidenced by the peaks from 1150 to 1000 cm^{-1}. The additional peak between 1750 and 1600 cm^{-1} is attributed to the presence of aldehydes, carboxylic acids, and ketones that
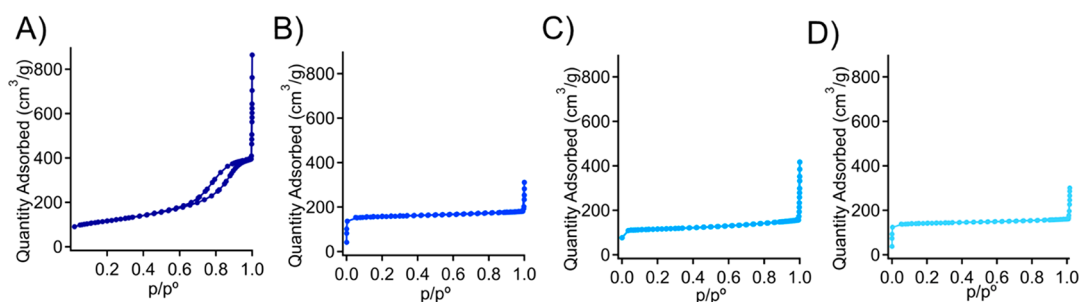
Figure 3. Nitrogen sorption isotherms (at 77 K) of carbonized mask fibers, which were cross-linked for (A) 2, (B) 4, (C) 6, and (D) 12 h.

are a result of side reactions during the sulfonation process. It was found that after 4 h, the FTIR spectra remain nearly constant, which suggests that the reaction is complete.

In addition to FTIR spectroscopy, the changes in the chemical composition of crosslinked PP fibers as a function of reaction time were investigated through XPS. Figure 1C depicts survey scans of the cross-linked fibers with an increasing sulfonation time. After reaction for 2 h, the low degree of sulfonation occurs with a limited increase in the levels of oxygen and sulfur to 3.3 atom % (at 532.23 eV) and 0.6 atom % (at 169.3 eV), respectively. Increasing the reaction time to 4 h resulted in significantly more pronounced peaks corresponding to these two heteroatoms. After sulfonation for 4 h, the oxygen and sulfur content reached plateau values at ~42.2% and ~9.7%, respectively, which slightly vary from those of a recent report (cross-linked at 120 °C) that exhibited oxygen and sulfur contents of 26% and 7%, respectively.[58] This discrepancy may be attributed to the faster reaction kinetics of PP in our study due to higher crosslinking temperatures employed. Further extending the reaction time resulted in a similar oxygen:sulfur ratio of ~4, which is consistent with previous reports.[59] Figure S1 includes high-resolution XPS scans for all cross-linked PP fibers. The oxygen:sulfur ratio of ~4 indicates that an additional oxygen-containing functionality is incorporated into the polymer for every sulfonic acid group that is attached to the backbone. This is likely due to side reactions that can form ketone species or other functional groups.

The heterogeneous sulfonation reaction results in some slight decreases in the diameter of the PP fibers, which were initially 17.8 μm. As the reaction progresses, the fiber diameter remained relatively constant around 14.5 μm. After the sulfonation-enabled cross-linking reaction, the fibers were washed and subsequently carbonized under a N_2 atmosphere at 800 °C. The cross-linking reaction enables carbon yields of ≤43% as depicted in Figure 2E. Specifically, sulfonation for 2 h resulted in a reduced carbon yield (~30%), which is similar to an observation from our previous work.[41] Shorter reaction times resulted in incomplete cross-linking of PP fibers, and the under-cross-linked fibers in the core regions were susceptible to thermal degradation. After sulfonation for 4 h, the carbon yield reaches a plateau at roughly 40%, confirming that cross-linking for 4 h using concentrated sulfuric acid at 145 °C is sufficient to fully cross-link the PP fibers in the mask samples. While this temperature was lower than the melting temperature of PPs (Figure S2), attached sulfonic acid groups on polymer backbones make PP become significantly more hydrophilic (Figure S3), which allows the efficient penetration of acid for further cross-linking. As shown in panels B−D and G−J of Figure 2, the fiber structures are completely maintained

throughout the vigorous cross-linking reaction and after carbonization. For all carbonized samples, the averaged fiber diameter is ~12 μm (Figure 2(G−J)), indicating an ~25% shrinkage from their original state. The reduced fiber diameter upon carbonization was slightly larger than those from multiple reports that used a similar process to produce carbon fibers from linear low-density PE.[60]

While fibril structures are maintained after cross-linking and carbonization steps, microporosity can be developed within PP-derived carbon. For example, several previous studies found that insufficient cross-linking from a short reaction time can result in hollow carbon fibers.[61] In this work, small diameters of PP fibers encouraged sufficient cross-linking within several hours. During the carbonization process, gaseous products were released through the decomposition of the cross-linked polymer fiber, which can induce porosity, as well as enhanced surface areas. Nitrogen sorption isotherms at 77 K were used to determine the pore characteristics of the carbonized fibers as a function of sulfonation time and are depicted in Figure 3. After sulfonation for 2 h (Figure 3A), lower degrees of sulfonation result in the formation of larger mesopores (Figure 3A) from un-crosslinked PP parts that are susceptible to thermal degradation. At longer sulfonation times, only micropores were present (Figure 3B−D) as a result of higher degrees of cross-linking. The carbonized PP fibers exhibit surface areas of 389, 486, 361, and 478 m^2/g after sulfonation for 2, 4, 6, and 12 h, respectively (Figure S4).

After carbonization, the heteroatom content of the carbon fibers was determined via XPS. Figure 4 depicts survey scans of the fibers that were carbonized after varying sulfonation times, and the corresponding heteroatom content of C, O, and S. Generally, the carbonization process results in the degradation of most heteroatom-containing functional groups while forming carbon frameworks. In our process, relatively high
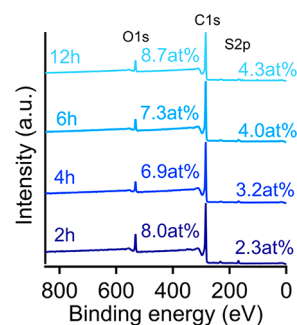
Figure 4. XPS survey scan spectra and heteroatom content of oxygen and sulfur in mask fibers after carbonization with varying cross-linking times.
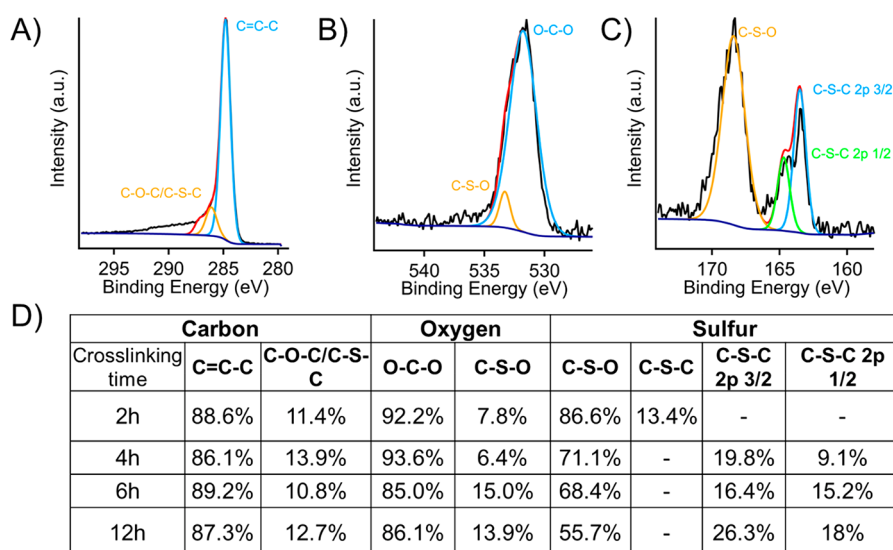
Figure 5. High-resolution XPS spectra and fitting results of (A) carbon, (B) oxygen, and (C) sulfur of carbon fiber masks, which were cross-linked for 6 h. (D) Relative ratios of peak intensity for each element in carbonized mask fibers after various cross-linking times.

	Carbon		Oxygen		Sulfur			
Crosslinking time	C=C-C	C-O-C/C-S-C	O-C-O	C-S-O	C-S-O	C-S-C	C-S-C 2p 3/2	C-S-C 2p 1/2
2h	88.6%	11.4%	92.2%	7.8%	86.6%	13.4%	-	-
4h	86.1%	13.9%	93.6%	6.4%	71.1%	-	19.8%	9.1%
6h	89.2%	10.8%	85.0%	15.0%	68.4%	-	16.4%	15.2%
12h	87.3%	12.7%	86.1%	13.9%	55.7%	-	26.3%	18%

levels of sulfur are incorporated into the carbon framework, resulting in oxygen, sulfur co-doped carbon fibers. Specifically, with an increased reaction time, we found that the sulfur content in the material increases while the oxygen content decreases. Carbon fibers that were initially sulfonated for 2 h exhibit heteroatom contents of 8 and 2.3 atom % for oxygen and sulfur, respectively. Increasing the reaction time to 6 and 12 h leads to oxygen contents of 7.3 and 8.7 atom % and sulfur contents of 4.0 and 4.3 atom %, respectively. Notably, the sulfur content of the carbon fibers in this system is increased compared to many instances in the literature using different doping methods.[58,62] However, it is comparable to that from studies of polyethylene-based precursors reacted under pressure, possibly suggesting that the increased sulfur content in the final product is a result of more vigorous reaction conditions. The presence of heteroatoms is anticipated to improve the performance of mask-derived carbon fibers for capture CO_2 due to their favorable interactions.

The heteroatom content of the materials (carbonized mask fibers) is further elucidated in the high-resolution XPS scans in Figure 5, during which the sample was cross-linked for 6 h. XPS results for other samples with different cross-linking times are included in Figure S5. Representative carbon, oxygen, and sulfur high-resolution scans are found in panels A−C, respectively, of Figure 5. The most predominant bond is the C═C−C found in Figure 5A, which corresponds to the conjugated framework of the carbonized fiber. Within the carbonized fiber, the most prevalent oxygen-containing functionality is represented by the C−O−C peak at 532.1 eV that represents epoxide groups. The high-resolution sulfur scan shows that most of the S atoms are represented by the peak at 168.4 eV, which corresponds to C−S−O bonds. Previously, oxidized sulfur-containing functional groups have been demonstrated to enhance the CO_2 adsorption performance of porous carbons due to their favorable interactions. As depicted in Figure 5D, the fibers that were cross-linked for 6 h exhibit the largest population of the C−S−O functional group when considering their increased content. Due to the largely similar pore characteristics of the samples depicted in this work, the effect of sulfur groups on the CO_2 adsorption of

masked derived carbon fibers can be observed in the CO_2 sorption isotherms in Figure 6.
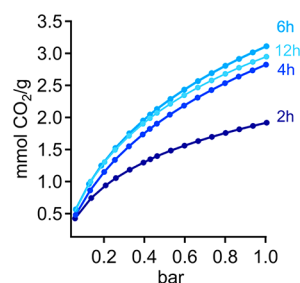
Figure 6. CO_2 adsorption isotherm at room temperature of carbonized mask fibers, which were crosslinked after varying times.

The porous nature and heteroatom content of the fibers enable their use as sorbents for CO_2 capture. Notably, the maximum specific sorption capacity exhibited by this system is 3.11 mmol/g at 1 bar (crosslinked for 6 h), which approaches those of some MOF or mesoporous carbon-based solid sorbents.[63,64] In comparison, a study performed by Seema et al. demonstrated an adsorption capacity of a S-doped microporous carbon as high as 4.0 mmol/g.[65] Similarly, various MOFs synthesized for CO_2 capture have adsorption capacities of >4 mmol/g.[66] While the sorption capacity of our mask-derived carbon fibers is slightly lower than these reported values, our technology employs waste plastics as feedback, paired with a simple and highly scalable process, suggesting its great commercial viability for addressing environmental threats of plastic waste and greenhouse gases. The sulfur heteroatoms were incorporated into the carbon precursors during the crosslinking reactions, a process that was significantly stream-lined compared to other doping methods. From our experimental measurements, the adsorption performance of mask-derived carbon fibers is directly related to the heteroatoms and chemical environments present in the carbon product. As previously discussed, the sample with the highest CO_2 adsorption capacity is the material produced after sulfonation for 6 h, which contains the largest amount of

oxidized S functional groups, providing favorable interactions between the polar CO_2 molecule and the porous carbon fibers. In addition to the excellent sorption capacity of the materials, they also exhibit a high selectivity toward CO_2 compared to N_2, which was determined through the use of Henry's law constants, where the selectivity ratio of CO_2 to N_2 was calculated by using the slope of each isotherm at pressures of <0.2 bar. These results illustrate that the amount of CO_2 that sorbents selectively adsorb is up to ~53 times the amount N_2 in a mixed process stream (Figure S6). While this is a model system, it demonstrates the potential to selectively adsorb CO_2 in practical situations that include mixed process streams containing nonpolar gas molecules like N_2 and CH_4.

Figure 6 shows that increasing the cross-linking time from 6 to 12 h results in a reduced CO_2 sorption capacity, while the derived carbon has a slightly higher sulfur content. This result suggests that the local chemical environment of sulfur atoms within the carbon framework is also important for determining the final CO_2 capture performance. To elucidate this important relationship, computational studies were performed to gain atomic-level insights into the enhanced CO_2 adsorption performance by S doping. As shown in Table 1, all but one

Table 1. Computed CO_2 Binding Energies for All of the Molecules Listed in Figure 7[a]

molecule (binding mode)	CO_2 binding energy (kcal/mol)	molecule (binding mode)	CO_2 binding energy (kcal/mol)
A0 (flat)	**−3.28**	**B0** (flat)	**−3.65**
A0 (vert)	−0.72	B0 (vert to flat)	−3.40
A1 (flat)	−2.90	B1 (flat)	−3.12
A1 (vert to flat)	**−3.53**	B1 (vert to flat)	−3.12
A2 (side)	**−4.38**	**B1** (side to flat)	**−3.18**
A3 (flat)	**−3.54**	B2 (flat)	−2.07
A3 (side)	−0.40	**B2** (vert to side)	**−5.39**
A4 (flat to side)	−5.47	B2 (side)	−4.96
A4 (side)	**−5.47**	B3 (flat)	−2.03
A5 (flat)	−4.94	B3 (vert)	−4.01
A5 (side)	**−5.06**	**B3** (side)	**−4.59**

[a]The strongest binding mode in each molecule is shown in bold. Binding modes are specified: flat, CO_2 molecule on the top of the aromatic ring plane and parallel; vert, CO_2 molecule on the top of the aromatic ring plane and vertical; side, CO_2 molecule on the side of the S-containing group. A change in binding modes (such as "vert to flat") indicates that the initial binding mode changed after geometry optimization.

(B1) S-containing molecule have a stronger affinity for CO_2 than their all-C counterparts. The largest increase in binding affinity is 2.19 kcal/mol or 67%, which occurs when A0 was modified to A4. These results confirmed that S doping can significantly enhance CO_2 binding, from the molecular level. Interestingly, molecules that have one S═O bond (A4 and B2) enhance CO_2 binding the most, compared to molecules that have none (A1, A3, and B1) or two (A5 and B3) S═O bonds. This result is consistent with our experimental observation, while suggesting that the CO_2 binding performance of these S-doped carbon fibers could be further optimized

by controlling the oxidation state of S in the doping experiments.

For the molecules without S═O bonds (A0, A1, A3, B0, and B1), the most favorable binding mode of the CO_2 molecule is always flat (Figure 7), which maximizes the dispersion interaction between CO_2 and the aromatic ring. The distance from the C atom in CO_2 to the aromatic ring plane is approximately 3.0−3.1 Å, close to the CO_2−benzene, CO_2−pyridine, and CO_2−pyrrole stacking structures reported in a previous study.[67] The O atoms in CO_2 that carry negative partial charges do not necessarily approach the S atoms that carry positive partial charges except in A1, indicating relatively weak electrostatic interactions. However, in molecules with one or two S═O bonds (A2, A4, A5, B2, and B3), the CO_2 molecules always prefer to adopt the side mode to bind close to the S═O bonds (Figure 7), potentially driven by the stronger electrostatic interactions because S═O bonds are much more polar than S−C and S−H bonds. Additionally, the C atom in CO_2 (carries a positive partial charge) is closer to the O atom in S═O bonds (carries a negative partial charge) in molecules that have one S═O bond (A4 and B2, ~2.55 Å) than in molecules containing two S═O bonds (A5 and B3, ~2.82 Å), leading to stronger electrostatic attraction. This result can potentially explain the aforementioned dependence of CO_2 binding affinity on the oxidation state of S. Also, A2 has weaker CO_2 binding than A4 or B2 despite also having one S═O bond because there is only C(CO_2)−O(ring) interaction but no O(CO_2)−S(ring) interaction, because the S atom in A2 is much more sterically hindered than the S atom in A4 and B2.

To better understand the physical nature of the CO_2 binding in different molecules, we performed energy decomposition analysis using the SAPT method for all of the A molecules. As shown in Table 2, the trends in total CO_2 binding energy from SAPT and DFT qualitatively agree with each other, in both of which A0 and A4 have the weakest and strongest binding to CO_2, respectively. More importantly, Table 2 also shows that the flat modes (A0, A1, and A3) are dominated by dispersion while side modes are dominated by electrostatics (A4 and A5), which confirms our aforementioned hypothesis. A2 is an exception as it can be seen as a combination of both side and flat (Figure 7). Collectively, the computational results provided important atomistic-level insights into the CO_2 binding process in the fibers and could shed light on the future design of carbon capture materials with even better performance.

Finally, the cycle stability of mask-derived carbon fibers for adsorption and desorption of CO_2 molecules was investigated to inform their long-term use and performance. Specifically, adsorption of CO_2 was accomplished at room temperature and 1 bar, while the desorption was performed by thermal treatment at increased temperatures. It was found that heating a sorbent at 150 °C can fully release captured CO_2 gas molecules, enabling the complete regeneration of spent sorbents (Figure S7). Additionally, the sorbents show an excellent cycle stability with >92% performance retention after >35 cycles. These results demonstrate that our simple method can be employed to convert PP-based mask waste into efficient CO_2 sorbents, which not only have high adsorption capacity and selectivity but also are recyclable for sustainable use.

4. CONCLUSIONS

In this study, carbon fibers derived from PP-based surgical masks were produced through cross-linking the polymer
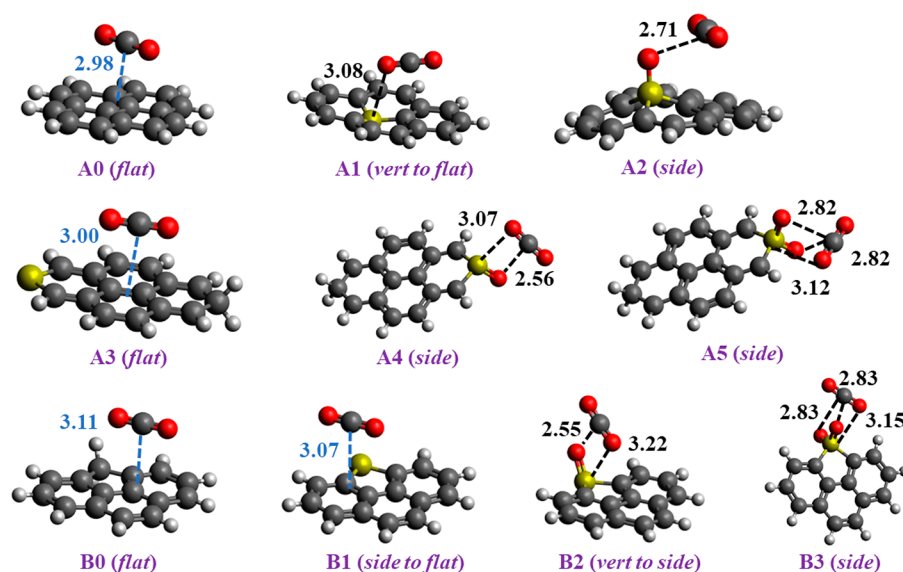
Figure 7. Optimized structures of the most favorable CO_2 binding mode for each molecule. Key atom−atom (black) and atom−plane (blue) interactions are shown in dashed lines along with the distance (in angstroms). Legend: H, white; C, gray; O, red; S, yellow.

Table 2. Results of SAPT-Based Energy Decomposition Analysis of the Most Favorable CO_2 Binding Mode for All A Molecules

molecule	electrostatics (kcal/mol)	dispersion (kcal/mol)	exchange (kcal/mol)	induction (kcal/mol)	total (SAPT) (kcal/mol)	total (DFT) (kcal/mol)
A0 (flat)	−3.27	−9.35	8.49	−1.08	−5.21	−3.28
A1 (vert to flat)	−3.28	−11.35	9.71	−1.62	−6.54	−3.53
A2 (side)	−6.46	−9.18	10.54	−1.57	−6.67	−4.38
A3 (flat)	−3.76	−9.15	8.46	−1.13	−5.58	−3.54
A4 (side)	−11.98	−6.43	13.05	−2.85	−8.21	−5.47
A5 (side)	−9.40	−6.02	10.89	−1.88	−6.41	−5.06

precursors in the presence of sulfuric acid at an increased temperature. The sulfonation reaction enables the incorporation of sulfur atoms into the carbon matrix, and upon variation of the sulfonation time, a controllable sulfur doping content in the carbon framework can be obtained (≤4.3 atom %). The presence of sulfur heteroatoms improves the CO_2 sorption capacity (≤3.11 mmol/g) and selectivity of carbon fibers due to their favorable polar interactions. Specifically, the effects of sulfur doping were analyzed through DFT and SAPT calculations, where binding energies of CO_2 were determined with regard to different local chemical environments. It was found that the structures with only one S═O bond formed the strongest binding interactions, in comparison to those with more than one S═O bond or without S═O bonds, which is consistent with our experimental observations. Overall, upcycling mask waste into sulfur-doped carbon fibers provides a simple and scalable alternative for producing CO_2 sorbents, while concurrently addressing the environmental challenges imposed by both greenhouse gases in the atmosphere and increased plastic pollution.

■ ASSOCIATED CONTENT

ⓢ Supporting Information

The Supporting Information is available free of charge at https://pubs.acs.org/doi/10.1021/acsaenm.2c00030.

Differential scanning calorimetry thermogram for a neat PP mask, water contact angle measurements for neat and sulfonated mask fibers, high-resolution XPS spectra for cross-linked and carbonized fibers, pore textures (surface areas, pore volumes, and pore size distributions) for the carbonized materials, CO_2/N_2 selectivity of the carbonized fibers, and CO_2 adsorption cycle stability (PDF)

■ AUTHOR INFORMATION

Corresponding Authors

Haoyuan Chen − *Department of Chemistry, The University of Texas Rio Grande Valley, Edinburg, Texas 78539, United States;* ⓞ orcid.org/0000-0002-8634-4028; Email: haoyuan.chen@utrgv.edu

Zhe Qiang − *School of Polymer Science and Engineering, The University of Southern Mississippi, Hattiesburg, Mississippi 39406, United States;* ⓞ orcid.org/0000-0002-3539-9053; Email: zhe.qiang@usm.edu

Authors

Mark Robertson − *School of Polymer Science and Engineering, The University of Southern Mississippi, Hattiesburg, Mississippi 39406, United States*

Alejandro Guillen Obando − *School of Polymer Science and Engineering, The University of Southern Mississippi, Hattiesburg, Mississippi 39406, United States*

Bianca Nunez − *Department of Chemistry, The University of Texas Rio Grande Valley, Edinburg, Texas 78539, United States*

Complete contact information is available at:
https://pubs.acs.org/10.1021/acsaenm.2c00030

■ REFERENCES

(1) Didenko, N. I.; Skripnuk, D. F.; Mirolyubova, O. v. Urbanization and Greenhouse Gas Emissions from Industry. *IOP Conf. Ser.: Earth Environ. Sci.* **2017**, *72*, 012014.

(2) D'Amato, G.; Vitale, C.; Lanza, M.; Molino, A.; D'Amato, M. Climate Change, Air Pollution, and Allergic Respiratory Diseases: An Update. *Curr. Opin. Allergy Clin. Immun.* **2016**, *16*, 434−440.

(3) D'Amato, G.; Cecchi, L.; D'Amato, M.; Annesi-Maesano, I. Climate Change and Respiratory Diseases. *Eur. Respir. Rev.* **2014**, *23*, 161−169.

(4) Overview of Greenhouse Gases. https://www.epa.gov/ghgemissions/overview-greenhouse-gases (accessed 2022-06-30).

(5) Creamer, A. E.; Gao, B. Carbon-Based Adsorbents for Postcombustion CO2 Capture: A Critical Review. *Environ. Sci. Technol.* **2016**, *50*, 7276−7289.

(6) The Paris Agreement. https://unfccc.int/process-and-meetings/the-paris-agreement/the-paris-agreement (accessed 2022-06−30).

(7) Sumida, K.; Rogow, D. L.; Mason, J. A.; McDonald, T. M.; Bloch, E. D.; Herm, Z. R.; Bae, T. H.; Long, J. R. Carbon Dioxide Capture in Metal-Organic Frameworks. *Chem. Rev.* **2012**, *112*, 724−781.

(8) Trickett, C. A.; Helal, A.; Al-Maythalony, B. A.; Yamani, Z. H.; Cordova, K. E.; Yaghi, O. M. The Chemistry of Metal−Organic Frameworks for CO2 Capture, Regeneration and Conversion. *Nat. Rev. Mater.* **2017**, *2*, 1−16.

(9) Karimi, M.; Shirzad, M.; Silva, J. A. C.; Rodrigues, A. E. Biomass/Biochar Carbon Materials for CO2 Capture and Sequestration by Cyclic Adsorption Processes: A Review and Prospects for Future Directions. *J. CO2 Util.* **2022**, *57*, 101890.

(10) Calvo-Muñoz, E. M.; García-Mateos, F. J.; Rosas, J. M.; Rodríguez-Mirasol, J.; Cordero, T. Biomass Waste Carbon Materials as Adsorbents for CO2 Capture under Post-Combustion Conditions. *Front. Mater.* **2016**, *3*, 23.

(11) Jiangfei, G.; Lizhi, W.; Zhang, D.; Huang, J. Amino-Functionalized Porphyrin-Based Porous Organic Polymers for CO 2 Capture and Hg 2+ Removal. *Energy Fuels* **2020**, *34*, 9771−9778.

(12) Bagherian, N.; Karimi, A. R.; Amini, A. Chemically Stable Porous Crystalline Macromolecule Hydrazone-Linked Covalent Organic Framework for CO2 Capture. *Colloids and Surf. A: Physicochem. Eng. Asp.* **2021**, *613*, 126078.

(13) Shen, Z.; Cai, Q.; Yin, C.; Xia, Q.; Cheng, J.; Li, X.; Wang, Y. Facile Synthesis of Silica Nanosheets with Hierarchical Pore Structure and Their Amine-Functionalized Composite for Enhanced CO2 Capture. *Chem. Eng. Sci.* **2020**, *217*, 115528.

(14) Dabbawala, A. A.; Ismail, I.; Vaithilingam, B. v.; Polychronopoulou, K.; Singaravel, G.; Morin, S.; Berthod, M.; al Wahedi, Y. Synthesis of Hierarchical Porous Zeolite-Y for Enhanced CO2 Capture. *Microporous Mesoporous Mater.* **2020**, *303*, 110261.

(15) Murge, P.; Dinda, S.; Roy, S. Zeolite-Based Sorbent for CO2 Capture: Preparation and Performance Evaluation. *Langmuir* **2019**, *35*, 14751−14760.

(16) Dunstan, M. T.; Donat, F.; Bork, A. H.; Grey, C. P.; Mü, C. R. CO2 Capture at Medium to High Temperature Using Solid Oxide-Based Sorbents: Fundamental Aspects, Mechanistic Insights, and Recent Advances. *Chem. Rev.* **2021**, *121*, 12681−12745.

(17) Jiménez, V.; Ramírez-Lucas, A.; Díaz, J. A.; Sánchez, P.; Romero, A. CO2 Capture in Different Carbon Materials. *Environ. Sci. Technol.* **2012**, *46*, 7407−7414.

(18) Hao, W.; Björkman, E.; Lilliestråle, M.; Hedin, N. Activated Carbons Prepared from Hydrothermally Carbonized Waste Biomass Used as Adsorbents for CO2. *Appl. Energy* **2013**, *112*, 526−532.

(19) Li, Q.; Liu, S.; Peng, W.; Zhu, W.; Wang, L.; Chen, F.; Shao, J.; Hu, X. Preparation of Biomass-Derived Porous Carbons by a Facile Method and Application to CO2 Adsorption. *J. Taiwan Inst. Chem. Eng.* **2020**, *116*, 128−136.

(20) Ma, X.; Su, C.; Liu, B.; Wu, Q.; Zhou, K.; Zeng, Z.; Li, L. Heteroatom-Doped Porous Carbons Exhibit Superior CO2 Capture and CO2/N2 Selectivity: Understanding the Contribution of Functional Groups and Pore Structure. *Sep. Purif. Technol.* **2021**, *259*, 118065.

(21) Saha, D.; Orkoulas, G.; Chen, J.; Hensley, D. K. Adsorptive Separation of CO2 in Sulfur-Doped Nanoporous Carbons: Selectivity and Breakthrough Simulation. *Microporous Mesoporous Mater.* **2017**, *241*, 226−237.

(22) Seredych, M.; Jagiello, J.; Bandosz, T. J. Complexity of CO2 Adsorption on Nanoporous Sulfur-Doped Carbons − Is Surface Chemistry an Important Factor? *Carbon* **2014**, *74*, 207−217.

(23) Tian, W.; Zhang, H.; Sun, H.; Suvorova, A.; Saunders, M.; Tade, M.; Wang, S. Heteroatom (N or N-S)-Doping Induced Layered and Honeycomb Microstructures of Porous Carbons for CO2 Capture and Energy Applications. *Adv. Funct. Mater.* **2016**, *26*, 8651−8661.

(24) Wang, Y.; Tian, Y.; Yan, L.; Su, Z. DFT Study on Sulfur-Doped g-C3N4 Nanosheets as a Photocatalyst for CO2 Reduction Reaction. *J. Phys. Chem. C* **2018**, *122*, 7712−7719.

(25) Ma, G.; Ning, G.; Wei, Q. S-Doped Carbon Materials: Synthesis, Properties and Applications. *Carbon* **2022**, *195*, 328−340.

(26) Climate Change and Municipal Solid Waste Fact Sheet | Pay-As-You-Throw. https://archive.epa.gov/wastes/conserve/tools/payt/web/html/factfin.html (accessed 2022-06-30).

(27) Naik, R. K.; Naik, M. M.; D'Costa, P. M.; Shaikh, F. Microplastics in Ballast Water as an Emerging Source and Vector for Harmful Chemicals, Antibiotics, Metals, Bacterial Pathogens and HAB Species: A Potential Risk to the Marine Environment and Human Health. *Mar. Pollut. Bull.* **2019**, *149*, 110525.

(28) Vollmer, I.; Jenks, M. J. F.; Roelands, M. C. P.; White, R. J.; van Harmelen, T.; de Wild, P.; van der Laan, G. P.; Meirer, F.; Keurentjes, J. T. F.; Weckhuysen, B. M. Beyond Mechanical Recycling: Giving New Life to Plastic Waste. *Angew. Chem., Int. Ed.* **2020**, *59*, 15402−15423.

(29) Zhang, F.; Wang, F.; Wei, X.; Yang, Y.; Xu, S.; Deng, D.; Wang, Y. Z. From Trash to Treasure: Chemical Recycling and Upcycling of Commodity Plastic Waste to Fuels, High-Valued Chemicals and Advanced Materials. *J. Energy Chem.* **2022**, *69*, 369−388.

(30) Easterling, C. P.; Kubo, T.; Orr, Z. M.; Fanucci, G. E.; Sumerlin, B. S. Synthetic Upcycling of Polyacrylates through Organocatalyzed Post-Polymerization Modification. *Chem. Sci.* **2017**, *8*, 7705−7709.

(31) Lewis, S. E.; Wilhelmy, B. E.; Leibfarth, F. A. Upcycling Aromatic Polymers through C−H Fluoroalkylation. *Chem. Sci.* **2019**, *10*, 6270−6277.

(32) Lee, Y. K.; Chung, S.; Hwang, S. Y.; Lee, S.; Eom, K. S.; Hong, S. B.; Park, G. G.; Kim, B. J.; Lee, J. J.; Joh, H. I. Upcycling of Lignin

Waste to Activated Carbon for Supercapacitor Electrode and Organic Adsorbent. *Korean J. Chem. Eng.* **2019**, *36*, 1543−1547.

(33) Choi, D.; Kil, H. S.; Lee, S. Fabrication of Low-Cost Carbon Fibers Using Economical Precursors and Advanced Processing Technologies. *Carbon* **2019**, *142*, 610−649.

(34) Villagómez-Salas, S.; Manikandan, P.; Acuña Guzman, S. F.; Pol, V. G. Amorphous Carbon Chips Li-Ion Battery Anodes Produced through Polyethylene Waste Upcycling. *ACS Omega* **2018**, *3*, 17520−17527.

(35) Wyss, K. M.; Beckham, J. L.; Chen, W.; Luong, D. X.; Hundi, P.; Raghuraman, S.; Shahsavari, R.; Tour, J. M. Converting Plastic Waste Pyrolysis Ash into Flash Graphene. *Carbon* **2021**, *174*, 430−438.

(36) Beckham, J. L.; Wyss, K. M.; Xie, Y.; McHugh, E. A.; Li, J. T.; Advincula, P. A.; Chen, W.; Lin, J.; Tour, J. M. Machine Learning Guided Synthesis of Flash Graphene. *Adv. Mater.* **2022**, *34*, 2106506.

(37) Chen, W.; Ge, C.; Li, J. T.; Beckham, J. L.; Yuan, Z.; Wyss, K. M.; Advincula, P. A.; Eddy, L.; Kittrell, C.; Chen, J.; Luong, D. X.; Carter, R. A.; Tour, J. M. Heteroatom-Doped Flash Graphene. *ACS Nano* **2022**, *16*, 6646−6656.

(38) Hu, X.; Lin, Z. Transforming Waste Polypropylene Face Masks into S-Doped Porous Carbon as the Cathode Electrode for Supercapacitors. *Ionics* **2021**, *27*, 2169−2179.

(39) Healthcare waste from COVID threatens environment. https://news.un.org/en/story/2022/02/1110982 (accessed 2022-06-30).

(40) Sullivan, G. L.; Delgado-Gallardo, J.; Watson, T. M.; Sarp, S. An Investigation into the Leaching of Micro and Nano Particles and Chemical Pollutants from Disposable Face Masks - Linked to the COVID-19 Pandemic. *Water Res.* **2021**, *196*, 117033.

(41) Robertson, M.; Güillen Obando, A.; Emery, J.; Qiang, Z. Multifunctional Carbon Fibers from Chemical Upcycling of Mask Waste. *ACS Omega* **2022**, *7*, 12278−12287.

(42) Yuan, X.; Li, S.; Jeon, S.; Deng, S.; Zhao, L.; Lee, K. B. Valorization of Waste Polyethylene Terephthalate Plastic into N-Doped Microporous Carbon for CO2 Capture through a One-Pot Synthesis. *J. Hazard. Mater.* **2020**, *399*, 123010.

(43) Algozeeb, W. A.; Savas, P. E.; Yuan, Z.; Wang, Z.; Kittrell, C.; Hall, J. N.; Chen, W.; Bollini, P.; Tour, J. M. Plastic Waste Product Captures Carbon Dioxide in Nanometer Pores. *ACS Nano* **2022**, *16*, 7284−7290.

(44) Zhao, Y.; Truhlar, D. G. The M06 Suite of Density Functionals for Main Group Thermochemistry, Thermochemical Kinetics, Noncovalent Interactions, Excited States, and Transition Elements: Two New Functionals and Systematic Testing of Four M06-Class Functionals and 12 Other Functionals. *Theor. Chem. Acc.* **2008**, *120*, 215−241.

(45) Weigend, F. Accurate Coulomb-Fitting Basis Sets for H to Rn. *Phys. Chem. Chem. Phys.* **2006**, *8*, 1057−1065.

(46) Grimme, S.; Ehrlich, S.; Goerigk, L. Effect of the Damping Function in Dispersion Corrected Density Functional Theory. *J. Comput. Chem.* **2011**, *32*, 1456−1465.

(47) Grimme, S.; Antony, J.; Ehrlich, S.; Krieg, H. A Consistent and Accurate Ab Initio Parametrization of Density Functional Dispersion Correction (DFT-D) for the 94 Elements H-Pu. *J. Chem. Phys.* **2010**, *132*, 154104.

(48) Boys, S. F.; Bernardi, F. The Calculation of Small Molecular Interactions by the Differences of Separate Total Energies. Some Procedures with Reduced Errors. *Mol. Phys.* **2006**, *19*, 553−566.

(49) Simon, S.; Duran, M.; Dannenberg, J. J. How Does Basis Set Superposition Error Change the Potential Surfaces for Hydrogen-bonded Dimers? *J. Chem. Phys.* **1996**, *105*, 11024.

(50) Weigend, F.; Ahlrichs, R. Balanced Basis Sets of Split Valence, Triple Zeta Valence and Quadruple Zeta Valence Quality for H to Rn: Design and Assessment of Accuracy. *Phys. Chem. Chem. Phys.* **2005**, *7*, 3297−3305.

(51) *Gaussian 16*; https://gaussian.com/gaussian16/ (accessed 2022-07-05).

(52) Jeziorski, B.; Moszynski, R.; Szalewicz, K. Perturbation Theory Approach to Intermolecular Potential Energy Surfaces of van Der Waals Complexes. *Chem. Rev.* **1994**, *94*, 1887−1930.

(53) Smith, D. G. A.; Burns, L. A.; Simmonett, A. C.; Parrish, R. M.; Schieber, M. C.; Galvelis, R.; Kraus, P.; Kruse, H.; Di Remigio, R.; Alenaizan, A.; James, A. M.; Lehtola, S.; Misiewicz, J. P.; Scheurer, M.; Shaw, R. A.; Schriber, J. B.; Xie, Y.; Glick, Z. L.; Sirianni, D. A.; O'Brien, J. S.; Waldrop, J. M.; Kumar, A.; Hohenstein, E. G.; Pritchard, B. P.; Brooks, B. R.; Schaefer, H. F.; Sokolov, A. Y.; Patkowski, K.; DePrince, A. E.; Bozkaya, U.; King, R. A.; Evangelista, F. A.; Turney, J. M.; Crawford, T. D.; Sherrill, C. D. PSI4 1.4: Open-Source Software for High-Throughput Quantum Chemistry. *J. Chem. Phys.* **2020**, *152*, 184108.

(54) Parker, T. M.; Burns, L. A.; Parrish, R. M.; Ryno, A. G.; Sherrill, C. D. Levels of Symmetry Adapted Perturbation Theory (SAPT). I. Efficiency and Performance for Interaction Energies. *J. Chem. Phys.* **2014**, *140*, 094106.

(55) Woon, D. E.; Dunning, T. H. Gaussian Basis Sets for Use in Correlated Molecular Calculations. III. The Atoms Aluminum through Argon. *J. Chem. Phys.* **1993**, *98*, 1358−1371.

(56) Kendall, R. A.; Dunning, T. H.; Harrison, R. J. Electron Affinities of the First-Row Atoms Revisited. Systematic Basis Sets and Wave Functions. *J. Chem. Phys.* **1992**, *96*, 6796−6806.

(57) Younker, J. M.; Saito, T.; Hunt, M. A.; Naskar, A. K.; Beste, A. Pyrolysis Pathways of Sulfonated Polyethylene, an Alternative Carbon Fiber Precursor. *J. Am. Chem. Soc.* **2013**, *135*, 6130−6141.

(58) Lee, G.; Eui Lee, M.; Kim, S. S.; Joh, H. I.; Lee, S. Efficient Upcycling of Polypropylene-Based Waste Disposable Masks into Hard Carbons for Anodes in Sodium Ion Batteries. *J. Ind. Eng. Chem.* **2022**, *105*, 268−277.

(59) Asthana, H.; Erickson, B. L.; Drzal, L. T. Sulfonation of Polymer Surfaces - II. Chemical Changes on Polypropylene and Polystyrene Surfaces after Gas Phase Sulfonation. *J. Adhes. Sci. Technol.* **1997**, *11*, 1269−1288.

(60) Eun, J. H.; Lee, J. S. Study on Polyethylene-Based Carbon Fibers Obtained by Sulfonation under Hydrostatic Pressure. *Sci. Rep.* **2021**, *11*, 18028.

(61) Hunt, M. A.; Saito, T.; Brown, R. H.; Kumbhar, A. S.; Naskar, A. K. Patterned Functional Carbon Fibers from Polyethylene. *Adv. Mater.* **2012**, *24*, 2386−2389.

(62) Qiang, Z.; Xia, Y.; Xia, X.; Vogt, B. D. Generalized Synthesis of a Family of Highly Heteroatom-Doped Ordered Mesoporous Carbons. *Chem. Mater.* **2017**, *29*, 10178−10186.

(63) Azmi, A. A.; Aziz, M. A. A. Mesoporous Adsorbent for CO2 Capture Application under Mild Condition: A Review. *J. Environ. Chem. Eng.* **2019**, *7*, 103022.

(64) Ghanbari, T.; Abnisa, F.; Wan Daud, W. M. A. A Review on Production of Metal Organic Frameworks (MOF) for CO2 Adsorption. *Sci. Total Environ.* **2020**, *707*, 135090.

(65) Seema, H.; Kemp, K. C.; Le, N. H.; Park, S. W.; Chandra, V.; Lee, J. W.; Kim, K. S. Highly Selective CO2 Capture by S-Doped Microporous Carbon Materials. *Carbon* **2014**, *66*, 320−326.

(66) Younas, M.; Rezakazemi, M.; Daud, M.; Wazir, M. B.; Ahmad, S.; Ullah, N.; Inamuddin; Ramakrishna, S. Recent Progress and Remaining Challenges in Post-Combustion CO2 Capture Using Metal-Organic Frameworks (MOFs). *Prog. Energy Combust. Sci.* **2020**, *80*, 100849.

(67) Chen, L.; Cao, F.; Sun, H. Ab Initio Study of the π−π Interactions between CO2 and Benzene, Pyridine, and Pyrrole. *Int. J. Quantum Chem.* **2013**, *113*, 2261−2266.